

# Slowly rotating Tolman VII solution

Camilo Posada and Zdeněk Stuchlík

Research Centre for Theoretical Physics and Astrophysics, Institute of Physics,  
Silesian University in Opava, Bezručovo nám. 13, CZ-746 01 Opava, Czech Republic

E-mail: [camilo.posada@physics.slu.cz](mailto:camilo.posada@physics.slu.cz) and [zdenek.stuchlik@physics.slu.cz](mailto:zdenek.stuchlik@physics.slu.cz)

## Abstract.

We present a model of a slowly rotating Tolman VII (T-VII) fluid sphere, at second order in the angular velocity. The structure of this configuration is obtained by integrating the Hartle-Thorne equations for slowly rotating relativistic masses. We model a sequence in adiabatic and quasi-stationary contraction, by varying the tenuity parameter  $R/R_S$ , where  $R$  is the radius of the configuration and  $R_S$  is its Schwarzschild radius. We determined the moment of inertia  $I$ , mass quadrupole moment  $Q$ , and the ellipticity  $\varepsilon$ , for various configurations. Similar to previous results for Maclaurin and polytropic spheroids, in slow rotation, we found a change in the behaviour of the ellipticity when the tenuity reaches a certain critical value. We compared our results of  $I$  and  $Q$  for the T-VII model with those predicted by the universal fittings proposed for realistic neutron stars. For the relevant range of compactness, we found that relative errors are within 10%, thus suggesting the T-VII solution as a very good approximation for the description of the interior of neutron stars.

*Keywords:* neutron stars, analytical solution, slow rotation, Hartle-Thorne metric.

## 1. Introduction

The study of the astrophysics of neutron stars (NSs) may provide key information, not only about the nuclear matter at extremely high densities (above nuclear saturation density) but also about the physics in the so-called strong gravity regime. A crucial element in this study is the equation of state (EOS), meaning the functional relation between pressure and mass-energy density of matter, which is commonly assumed to be described by a perfect fluid. Although various reasonable tabulated EOSs for realistic NSs have been proposed in the literature (see e.g. [1]), a definitive relation that can describe satisfactorily the internal constitution of NSs remains one of the biggest puzzles in relativistic astrophysics.

Finding solutions to Einstein's equations, given certain EOS, is useful to connect observables like mass, radii, Love numbers, etc., with the NS internal structure. For instance, one alternative is to study configurations with polytropic EOS [2, 3, 4] and simulate the realistic EOS by sequences of polytropic configurations [5, 6]. However, most of these solutions must be computed numerically due to the complexity of the field equations. Another alternative is to find analytic solutions to Einstein's equations

that can describe, approximately, the interior structure of NSs. In this context, Schwarzschild's interior solution for an incompressible fluid [7, 8, 9], the Buchdahl model [10], and the Tolman VII (T-VII) solution [11], have been commonly employed in the study of the interior properties of NSs [12, 13], and also in the context of the so-called  $I$ -Love- $Q$  relations [14, 15]. The T-VII solution is characterized by possessing an energy density that varies quadratically with the radial coordinate; this behaviour turns out to be eminently reasonable for the intermediate regions of realistic NSs [12], the reason why the T-VII model has attracted considerable interest in the literature [16, 17, 18, 19, 20, 21, 22, 23, 24, 25, 26, 27, 28, 29, 30, 31].

Recent measurements carried out by the Neutron Star Interior Composition Explorer (NICER) [32], have placed important constraints on values of masses and radii of rotation-powered X-ray pulsars [33, 34, 35]. Thus, the study of the rotational properties of compact objects is of great interest, and numerous approaches have been proposed in the context of GR [36]. One of them is the perturbative method for slowly rotating relativistic masses, up to second order in the rotational speed  $\Omega$ , developed by Hartle and Thorne (HT) [37, 38]. In this approach, a static and spherically symmetric background configuration with mass  $M$  and radius  $R$  is set into slow uniform rotation, such that,  $\delta = \Omega/\Omega_0 \ll 1$ , where,  $\Omega_0 = \sqrt{GM/4\pi^2 R^3}$  is the mass-shedding frequency. Thus, fractional changes in pressure, energy density, and gravitational field are much less than unity. The slowly rotating approximation is reasonable for most of the known pulsars with  $\Omega < 300$  Hz, for instance, PSR J0030+0451, whose frequency was estimated to be  $f = 205.53$  Hz, so  $\delta = 0.14$  [39]. Even for PSR J0740 + 6620, which spins at 346.53 Hz [40],  $\delta \sim 0.16$  thus validating the slowly rotating approximation.

The HT formalism has been applied to various tabulated EOSs for NSs, since their pioneering work [38] and more recently by [39]. In the context of solutions to Einstein's equations for compact objects, the HT perturbative method has been applied to uniform density configurations [41, 42, 43] and polytropic fluid spheres [44, 45]. A slowly rotating T-VII model was considered by [23, 26], but only to the leading order in the perturbation; however, a full treatment to the second order in  $\Omega$  is still missing. Thus, motivated by the developments discussed above, in this paper, we present an extension to slow rotation of the T-VII solution, by solving the HT structure equations at the second order in the angular frequency  $\Omega$ .

The organization of the paper is as follows. In section 2 we review the perturbative HT method for slowly rotating relativistic masses, at the second order in the angular frequency  $\Omega$ . In section 3 we discuss briefly the T-VII solution. In section 4 we present our numerical results for the integral and surface properties of slowly rotating T-VII fluid spheres. In section 5 we draw our concluding remarks.

*Conventions and notation:* We use geometrized units ( $c = G = 1$ ), unless stated otherwise, and we adopt the signature  $(-, +, +, +)$  for the metric.

## 2. Hartle-Thorne framework for slowly rotating relativistic stars

In this section, we review the HT method for slowly rotating relativistic masses [37, 38]. We follow the notation and conventions used in [38, 41, 44].

### 2.1. Non-rotating configuration in hydrostatic equilibrium

The starting point is a non-rotating configuration which is described by a metric in the spherically symmetric Schwarzschild-like form

$$ds^2 = -e^{\nu(r)} dt^2 + e^{\lambda(r)} dr^2 + r^2(d\theta^2 + \sin^2\theta d\phi^2), \quad (2.1)$$

where

$$e^{-\lambda(r)} \equiv 1 - \frac{2m(r)}{r}, \quad m(r) = 4\pi \int_0^r \epsilon(r) r^2 dr. \quad (2.2)$$

Here  $\epsilon$  is the energy density and  $m(r)$  denotes the mass enclosed by the radius  $r$ . The total gravitational mass of the configuration is given by  $M = m(R)$ . Given a value of the central energy density  $\epsilon_c$ , the non-rotating configuration is determined by integrating the Tolman-Oppenheimer-Volkoff (TOV) equation of hydrostatic equilibrium,

$$\frac{dp}{dr} = -(\epsilon + p) \frac{m(r) + 4\pi pr^3}{r[r - 2m(r)]}, \quad (2.3)$$

together with the equation for the time metric component  $e^{\nu(r)}$  given by

$$\frac{d\nu}{dr} = -\frac{2}{(\epsilon + p)} \left( \frac{dp}{dr} \right). \quad (2.4)$$

In the exterior vacuum spacetime  $\epsilon = p = 0$ , thus the geometry is described by the Schwarzschild metric

$$e^{\nu(r)} = e^{-\lambda(r)} = 1 - \frac{2M}{r}, \quad r > R. \quad (2.5)$$

The interior and exterior geometries are matched across the boundary  $\Sigma_0 = R$

$$[\lambda] = 0, \quad [\nu] = 0, \quad [\nu'] = 0, \quad (2.6)$$

where  $[f]$  indicates the difference between the value of  $f$  in the vacuum exterior and its value in the interior, evaluated at  $\Sigma_0$ , i.e.,  $[f] = f^+|_{\Sigma_0} - f^-|_{\Sigma_0}$ , and the prime denotes derivative with respect to the radial coordinate  $r$   $\ddagger$ .

### 2.2. Hartle-Thorne equations for the rotational metric deformations

Once the equilibrium configuration is set into slow rotation, the interior distribution and the spacetime geometry around it change. Thus, the appropriate line element for this situation is [37, 38]

$$\begin{aligned} ds^2 = & -e^{\nu} [1 + 2h_0(r) + 2h_2(r)P_2(\cos\theta)] dt^2 \\ & + e^{\lambda} \left\{ 1 + \frac{e^{\lambda}}{r} [2m_0(r) + 2m_2(r)P_2(\cos\theta)] \right\} dr^2 \\ & + r^2 [1 + 2(v_2 - h_2)P_2(\cos\theta)] [d\theta^2 + \sin^2\theta(d\phi - \omega dt)^2], \end{aligned} \quad (2.7)$$

$\ddagger$  We use the opposite convention of [43], who uses  $+(-)$  to denote quantities in the interior (exterior).

where  $P_2(\cos \theta)$  is the Legendre polynomial of order 2;  $(h_0, h_2, m_0, m_2, v_2)$  are quantities of order  $\Omega^2$ ; and  $\omega(r)$  corresponds to the angular velocity of the local inertial frame, relative to a distant observer. The function  $\omega(r)$  is associated with the *dragging* effect. Note that in the non-rotating case, the metric (2.7) reduces to (2.1).

We assume the fluid, inside the configuration, rotating uniformly with four-velocity  $u^\mu$  given by

$$\begin{aligned} u^t &= (-g_{tt} - 2\Omega g_{t\phi} - g_{\phi\phi}\Omega^2)^{-1/2} \\ &= e^{-\nu/2} \left[ 1 + \frac{1}{2}r^2 \sin^2 \theta (\Omega - \omega)^2 e^{-\nu} - h_0 - h_2 P_2 \right], \\ u^\phi &= \Omega u^t, \quad u^r = u^\theta = 0. \end{aligned}$$

It is conventional to introduce the quantity

$$\varpi \equiv \Omega - \omega, \quad (2.8)$$

which corresponds to the angular velocity of the fluid relative to the local inertial frame. This quantity determines the centrifugal force and, at first order in  $\Omega$ , satisfies the following equation

$$\frac{d}{dr} \left[ r^4 j(r) \frac{d\varpi}{dr} \right] + 4r^3 \frac{dj}{dr} \varpi = 0, \quad j(r) \equiv e^{-(\lambda+\nu)/2}. \quad (2.9)$$

In the region  $r > R$ ,  $\epsilon = p = 0$  and the space-time geometry is described by (2.5). Thus,  $j(r) = 1$  and (2.9) can be easily integrated to give

$$\varpi(r)^+ = \Omega - \frac{2J}{r^3}, \quad (2.10)$$

where  $J$  is an integration constant associated with the angular momentum of the star [37]. For the interior solution, (2.9) is integrated outward from the origin, with the boundary conditions  $\varpi(0) = \varpi_c = \text{const.}$ , and  $(d\varpi/dr)|_{r=0} = 0$ . Regularity demands that, at the surface, the interior and exterior solutions, together with their derivatives, must match, i.e.,  $[\varpi] = [\varpi'] = 0$ . Thus, one integrates numerically (2.9) and obtains the surface value  $\varpi(R)$ , then one can determine the angular momentum  $J$  and the angular velocity  $\Omega$  as follows

$$J = \frac{1}{6}R^4 \left( \frac{d\varpi}{dr} \right)_{r=R}, \quad \Omega = \varpi(R) + \frac{2J}{R^3}. \quad (2.11)$$

Once the angular momentum and angular velocity are determined, the relativistic moment of inertia can be obtained by the relation  $I = J/\Omega$ .

### 2.3. Spherical deformations: $l = 0$ sector

The spherical deformations are determined by the  $l = 0$  equations, for the perturbations  $m_0$  and  $p_0^*$ , which read

$$\frac{dm_0}{dr} = 4\pi r^2 (\epsilon + p) \left( \frac{d\epsilon}{dp} \right) p_0^* + \frac{1}{12} r^4 j^2 \left( \frac{d\varpi}{dr} \right)^2 - \frac{1}{3} r^3 \varpi^2 \frac{dj^2}{dr}, \quad (2.12)$$

$$\begin{aligned} \frac{dp_0^*}{dr} = & -\frac{1+8\pi pr^2}{(r-2m)^2}m_0 - \frac{4\pi(\epsilon+p)r^2}{r-2m}p_0^* + \frac{1}{12}\frac{r^4j^2}{(r-2m)}\left(\frac{d\varpi}{dr}\right)^2 \\ & + \frac{1}{3}\frac{d}{dr}\left(\frac{r^3j^2\varpi^2}{r-2m}\right). \end{aligned} \quad (2.13)$$

These equations are integrated outward, from the origin, with the boundary conditions  $h_0(0) = m_0(0) = 0$ . In the exterior of the star, (2.12) and (2.13) are integrated explicitly giving

$$m_0^+(r) = \delta M - \frac{J^2}{r^3}, \quad (2.14)$$

$$h_0^+(r) = -\frac{\delta M}{r-2M} + \frac{J^2}{r^3(r-2M)}, \quad (2.15)$$

where  $\delta M$  is an integration constant that is associated with the change in mass induced by the rotation, and it can be found by the matching of the solutions at the surface  $\Sigma_0$ , i.e.,  $[m_0] = [h_0] = 0$ .

As it was pointed out by [46], expression (2.14) for  $\delta M$  is not the most general one. By reconsidering the matching problem in the HT framework, by employing the perturbed matching theory at second order developed by [47], [46] showed that the perturbative functions are continuous across the surface  $\Sigma_0$ , except for the function  $m_0(r)$  in the  $l=0$  sector. The discontinuity in  $m_0(r)$  turns out to be proportional to the energy density at  $\Sigma_0$ , thus contributing an additional term to (2.14) in the form

$$\delta M_{\text{mod}} = m_0(R) + \frac{J^2}{R^3} + 8\pi R^3 \left( \frac{R}{2M} - 1 \right) \epsilon(R) p_0^*. \quad (2.16)$$

Note that for configurations with a vanishing surface energy density, as is the case for most of the EOS for realistic NSs including the T-VII solution, this additional term vanishes; thus the original HT expression (2.14) remains valid. However, for configurations with a discontinuity in  $\epsilon$  at the surface, e.g. constant density stars or strange stars [48], this additional term provides a significant contribution to the change in mass [43].

#### 2.4. Quadrupole deformations: $l=2$ sector

The quadrupole deformations of the star are determined by the  $l=2$  perturbations equations given by

$$\begin{aligned} \frac{dh_2}{dr} = & \left\{ -\frac{d\nu}{dr} + \frac{r}{(r-2m)} \left( \frac{d\nu}{dr} \right)^{-1} \left[ 8\pi(\epsilon+p) - \frac{4m}{r^3} \right] \right\} h_2 \\ & - \frac{4v_2}{r(r-2m)} \left( \frac{d\nu}{dr} \right)^{-1} + \frac{1}{6} \left[ \frac{r}{2} \left( \frac{d\nu}{dr} \right) - \frac{1}{(r-2m)} \left( \frac{d\nu}{dr} \right)^{-1} \right] r^3 j^2 \left( \frac{d\varpi}{dr} \right)^2 \\ & - \frac{1}{3} \left[ \frac{r}{2} \left( \frac{d\nu}{dr} \right) + \frac{1}{(r-2m)} \left( \frac{d\nu}{dr} \right)^{-1} \right] r^2 \frac{dj^2}{dr} \varpi^2, \end{aligned} \quad (2.17)$$

$$\frac{dv_2}{dr} = - \left( \frac{d\nu}{dr} \right) h_2 + \left( \frac{1}{r} + \frac{1}{2} \frac{d\nu}{dr} \right) \left[ \frac{1}{6} r^4 j^2 \left( \frac{d\varpi}{dr} \right)^2 - \frac{1}{3} r^3 \varpi^2 \frac{dj^2}{dr} \right]. \quad (2.18)$$

The solutions of (2.17) and (2.18) can be expressed as the sum of a homogenous part and a particular solution

$$h_2 = Ah_2^h + h_2^p, \quad v_2 = Av_2^h + v_2^p, \quad (2.19)$$

where the particular solution is given by the integration of (2.17) and (2.18), with the following near-the-origin behaviours

$$h_2^p = ar^2, \quad v_2^p = br^2, \quad (2.20)$$

where, for an arbitrary value of  $a$ , the constant  $b$  satisfies the following constraint [41, 44]

$$b = \frac{2\pi}{3} [(\epsilon_c + p_c)j_c^2 - (\epsilon_c + 3p_c)a]. \quad (2.21)$$

On the other hand, the homogenous integrals are obtained from the following equations

$$\frac{dv_2^h}{dr} = - \left( \frac{d\nu}{dr} \right) h_2^h, \quad (2.22)$$

$$\begin{aligned} \frac{dh_2^h}{dr} = & - \left\{ \frac{d\nu}{dr} - \frac{r}{(r-2m)} \left( \frac{d\nu}{dr} \right)^{-1} \left[ 8\pi(\epsilon + p) - \frac{4m}{r^3} \right] \right\} h_2^h \\ & - \frac{4v_2^h}{r(r-2m)} \left( \frac{d\nu}{dr} \right)^{-1}. \end{aligned} \quad (2.23)$$

These equations are integrated outward from the center of the star where they behave as follows

$$h_2^h = Br^2, \quad v_2^h = -\frac{2\pi}{3} (\epsilon_c + 3p_c) Br^4, \quad (2.24)$$

where  $B$  is an arbitrary constant. In the vacuum exterior, (2.17) and (2.18) can be integrated analytically to give

$$h_2^+(r) = J^2 \left( \frac{1}{Mr^3} + \frac{1}{r^4} \right) + KQ_2^2 \left( \frac{r}{M} - 1 \right), \quad (2.25)$$

$$v_2^+(r) = -\frac{J^2}{r^4} + K \frac{2M}{[r(r-2M)]^{1/2}} Q_2^1 \left( \frac{r}{M} - 1 \right), \quad (2.26)$$

where  $K$  is an integration constant, and  $Q_n^m$  are the associated Legendre functions of the second kind. The condition of regularity of the solutions at the surface  $\Sigma_0$  demands  $[h_2] = [v_2] = 0$ . The constant  $K$  appearing in Eqs. (2.25) and (2.26), is related to the quadrupole mass moment of the star, as measured at infinity, via the relation

$$Q = \frac{J^2}{M} + \frac{8}{5} KM^3. \quad (2.27)$$

To find the constant  $K$ , the functions  $h_2$  and  $v_2$  must be computed for the interior of the star, and then matched at the surface  $\Sigma_0$  with the exterior solutions (2.25) and (2.26).

The perturbations for mass and pressure  $m_2$  and  $p_2^*$ , which determine the rotational deformations of the star, can be determined using the following relations [38]

$$m_2 = (r - 2m) \left[ -h_2 - \frac{1}{3}r^3 \left( \frac{dj^2}{dr} \right) \varpi^2 + \frac{1}{6}r^4 j^2 \left( \frac{d\varpi}{dr} \right)^2 \right], \quad (2.28)$$

$$p_2^* = -h_2 - \frac{1}{3}r^2 e^{-\nu} \varpi^2. \quad (2.29)$$

The equation that describes the isobaric surfaces can be written as [41, 44]

$$r(p) = r_0 + \xi_0(r) + \xi_2(r)P_2(\cos \theta), \quad (2.30)$$

where  $r_0$  is the radius of the nonrotating configuration, and where the pressure has value  $p$ . The deformations are given by

$$\xi_0(r) = -p_0^*(\epsilon + p) \left( \frac{dp}{dr} \right)^{-1}, \quad (2.31)$$

$$\xi_2(r) = -p_2^*(\epsilon + p) \left( \frac{dp}{dr} \right)^{-1}. \quad (2.32)$$

Equation (2.30) is written in a particular coordinate system. However, one can construct an invariant parametrization of the isobaric surface by embedding it in a three-dimensional flat space with polar coordinates  $r^*, \theta^*, \phi^*$  which has the same intrinsic geometry as the isobaric surface. Thus, the corresponding 3-surface in flat space (at order  $\Omega^2$ ) is given by

$$r^*(\theta^*) = r_0 + \xi_0(r) + [\xi_2 + r(v_2 - h_2)]P_2(\cos \theta). \quad (2.33)$$

The ellipticity of this spheroid is given by [44]

$$\varepsilon = -\frac{3}{2r} [\xi_2 + r(v_2 - h_2)]. \quad (2.34)$$

Miller [44] has shown that there is an alternative way to define ellipticity using proper distances. However, in the following, we use the definition given by (2.34).

### 3. Tolman VII fluid spheres

In this section, we review the T-VII solution [11, 12, 25]. In his prescription, Tolman assumed the radial metric component  $g_{rr} = e^{\lambda(r)}$  in the form

$$e^{-\lambda(r)} = 1 - \frac{\xi^2}{2\beta}(5 - 3\xi^2), \quad (3.1)$$

where  $\xi \equiv r/R$  is the radial coordinate normalized by the stellar radius, and  $\beta \equiv R/R_S$ , where  $R_S (= 2M)$  is the Schwarzschild radius, denotes the ‘tenuity’ parameter [16]. In contrast with [12, 25], instead of the compactness  $\mathcal{C} \equiv M/R$ , here we parametrize the T-VII solution by the tenuity  $\beta$ . Both quantities are connected via the relation  $\mathcal{C} = 1/(2\beta)$ .

The remaining functions describing the T-VII solution are given as follows: the energy density  $\epsilon$  follows a quadratic fall-off form, as a function of  $r$ , given by

$$\epsilon(\xi) = \epsilon_c(1 - \xi^2), \quad (3.2)$$

where  $\epsilon_c$  indicates the central energy density. Note that  $\epsilon$  vanishes at the surface  $\xi = 1$ . From (2.2) we obtain the mass enclosed by the radius  $r$  as

$$m(\xi) = \frac{M}{2}\xi^3(5 - 3\xi^2), \quad (3.3)$$

which gives the total gravitational mass  $M$  when evaluated at the surface  $\xi = 1$ . On the other hand, the  $g_{tt}$  metric component results

$$e^\nu = C_1 \cos^2 \phi(\xi), \quad (3.4)$$

where

$$\phi(\xi) = C_2 - \frac{1}{2} \log \left( \xi^2 - \frac{5}{6} + \sqrt{\frac{2\beta}{3e^\lambda}} \right), \quad (3.5)$$

and  $C_1$  and  $C_2$  are integration constants given by

$$C_1 = 1 - \frac{5}{6\beta},$$

$$C_2 = \arctan \sqrt{\frac{1}{6(\beta - 1)}} + \frac{1}{2} \log \left( \frac{1}{6} + \sqrt{\frac{2(\beta - 1)}{3}} \right).$$

Finally, the radial pressure is found to be

$$p(\xi) = \frac{\epsilon_c}{15} \left[ \sqrt{24\beta e^{-\lambda}} \tan \phi - (5 - 3\xi^2) \right], \quad (3.6)$$

which vanishes at the surface  $\xi = 1$ . With the help of (3.2) and (3.3), we can find a relation between the tenuity and the central energy density as

$$\epsilon_c = \frac{15}{16\pi\beta R^2}. \quad (3.7)$$

Let us recall certain restrictions, on the parameter  $\beta$ , for the physical plausibility of the T-VII solution. The central pressure is finite for  $\beta > 1.2946$ , which is above the lower tenuity allowed by the Buchdahl theorem (valid for any EOS), namely,  $\beta \geq 9/8$  [49]. On the other hand, the dominant energy condition (DEC), which demands that the pressure should not exceed the energy density, i.e.,  $\epsilon > |p|$ , is valid for  $\beta > 1.4921$  [25]. Causality, as determined by the condition that the central speed of sound,  $c_s(0) = \sqrt{(\partial p / \partial \epsilon)|_{\xi=0}} \leq 1$ , is valid up to  $\beta = 1.8540$ . In figure 1 we show the profiles of the speed of sound  $c_s$ , for different values of the tenuity parameter  $\beta$ , as a function of the radial coordinate  $\xi$ . Note that  $c_s$  is maximum at the centre and decreases monotonically with  $r$ , going to zero at the surface. Additionally, the T-VII solution is stable, against radial oscillations, for  $\beta > 1.4585$  [20, 25]. We summarize these bounds in table 1.

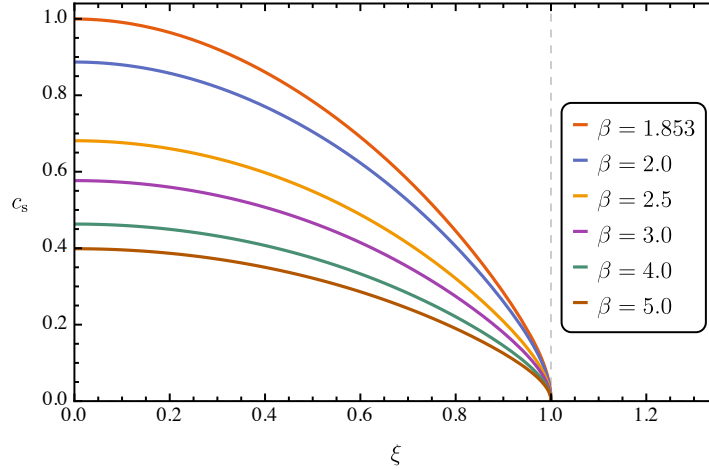


**Figure 1.** Profiles of the speed of sound  $c_s = \sqrt{(\partial p / \partial \epsilon)}$ , as a function of the radial coordinate  $\xi$ , for the T-VII solution. The various curves shown here correspond to different values of the tenuity parameter  $\beta$ .

**Table 1.** Limits on the tenuity  $\beta$  for the physical viability of the T-VII spheres, as determined by the following conditions: (a) finite ratio  $p_c/\epsilon_c$ , (b) radial stability, (c) dominant energy condition, and (d) causality.

Condition	$\beta$
Finite $p_c/\epsilon_c$	1.2946
Stability	1.4585
DEC	1.4921
$c_s(0) \leq 1$	1.8532

#### 4. Numerical results for slowly rotating T-VII spheres

In this section, we present our results of the numerical integrations of the HT structure equations, for slowly rotating T-VII fluid spheres, up to the second order in the angular velocity  $\Omega$ . The HT equations were integrated for various values of the tenuity parameter  $\beta$ , up to the limiting value for dynamical stability  $\beta_{\text{stab}}$  (see table 1), using a standard fourth-order Runge-Kutta algorithm. Although the limits on  $\beta$  as given by the DEC and sub-luminal central speed of sound are stricter than those given by the dynamical stability condition, we consider the latter as our limiting tenuity during the integration. Since the ratio  $J/M^2$  is conserved in a quasi-stationary and semi-adiabatic collapse (to the order of the approximation), we assume it constant during the integrations (see discussion in [44]). In table A1 we list some of the properties of the models evaluated at the surface. The main results of the integrations are presented further in figures 2-10. Following [41, 44] we use dimensionless variables where the units in which the quantities are expressed, are given in the corresponding descriptions.

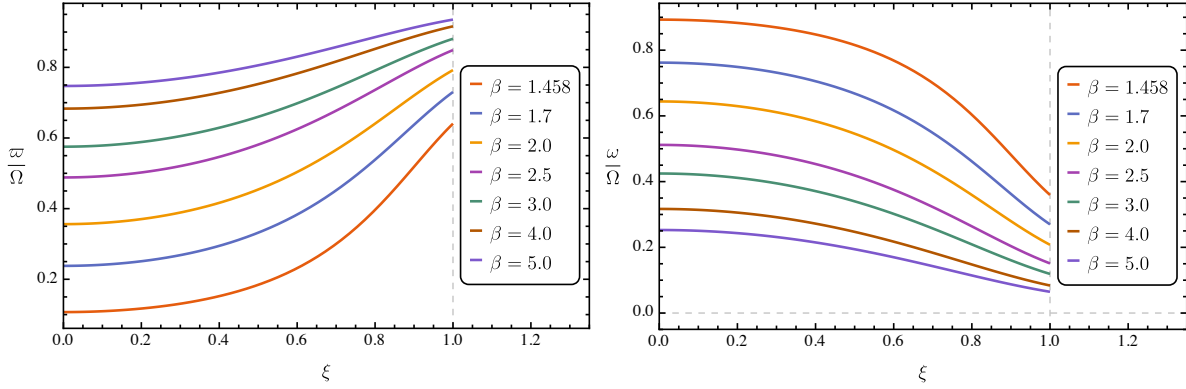


**Figure 2.** *Dragging of the inertial frames.* **Left panel:** radial profile of the angular velocity  $\varpi/\Omega = (1 - \omega/\Omega)$ , relative to the local inertial frame (as measured by a distant observer), for the T-VII solution. We normalize  $\varpi$  by the fluid’s angular velocity  $\Omega$  relative to a distant observer. The curves are labelled by their corresponding values of  $\beta$ . **Right panel:** angular velocity  $\omega/\Omega$ , or dragging of the inertial frames, as a function of the radial coordinate  $\xi$ . We show profiles for the same values of  $\beta$  as in the right-hand panel. We normalize  $\omega$  by the fluid’s angular velocity  $\Omega$  relative to a distant observer. Note that the dragging is maximum at the centre of the star, and it decreases outwards.

#### 4.1. Dragging of inertial frames and moment of inertia

The dragging of the inertial frames, in the T-VII space-time, can be studied from figure 2. In the left-hand panel, we plot the radial profile of  $\varpi(r)$ , corresponding to the angular velocity of the fluid relative to the local inertial frame, for different values of the tenuity  $\beta$ . We observe that  $\varpi$  has a local minimum at the origin, and it grows monotonically with  $r$  up to the surface  $\xi = 1$ . Therefore, the dragging of inertial frames, as measured by a distant observer, is greatest at the origin of the star and it decreases outward, as is also shown in the right-hand panel of the same figure. We also observe that as the tenuity decreases, i.e. the star becomes more compact, the  $\varpi(r)$  function is suppressed, while the ‘dragging function’  $\omega(r)$  is enhanced. Thus, the more compact the configuration, the greater the dragging of local inertial frames in the interior of it. For the limiting value  $\beta_{\text{stab}}$ , for dynamical stability, the central value of  $\varpi$  is close to zero, but it does not vanish, in agreement with a theorem due to [37].

In figure 3 we show the surface value of  $\varpi_1$ , relative to the local inertial frame, as a function of the tenuity  $\beta$ . We observe that as the compactness of the star increases,  $\varpi_1$  increases, reaching a local maximum at  $\beta \simeq 1.51$  and then it decreases. Similar behaviour was found for configurations with uniform density in slow rotation, although the maximum there appears at  $\beta \simeq 1.43$  [41].

The left-hand panel of figure 4 displays the dimensionless moment of inertia  $\tilde{I} \equiv I/M^3$ , as a function of the tenuity  $\beta$ . The quantity  $\tilde{I}$  has been shown to be relevant in the context of the  $I$ -Love- $Q$  [5, 14], and  $I$ -Love- $\mathcal{C}$  relations [23]. First of all, we confirmed the results reported by [23] for the T-VII solution. We observe that  $\tilde{I}$  decreases monotonically, and seems to approach the black hole (BH) limit  $\tilde{I}_{\text{BH}} = 4$ ,

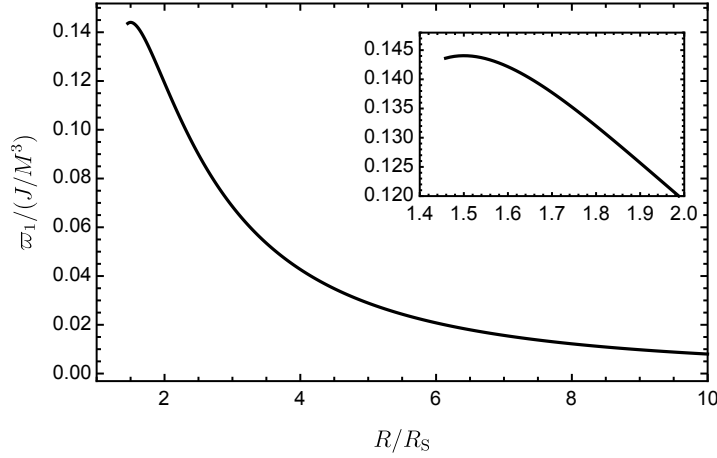


**Figure 3.** Surface value of the angular velocity  $\varpi_1$ , relative to the local inertial frame, for different values of the tenuity parameter  $R/R_S$ , for T-VII spheres. We measure  $\varpi_1$  in units of  $J/M^3$ . The inset shows a magnification in the region near the local maximum.

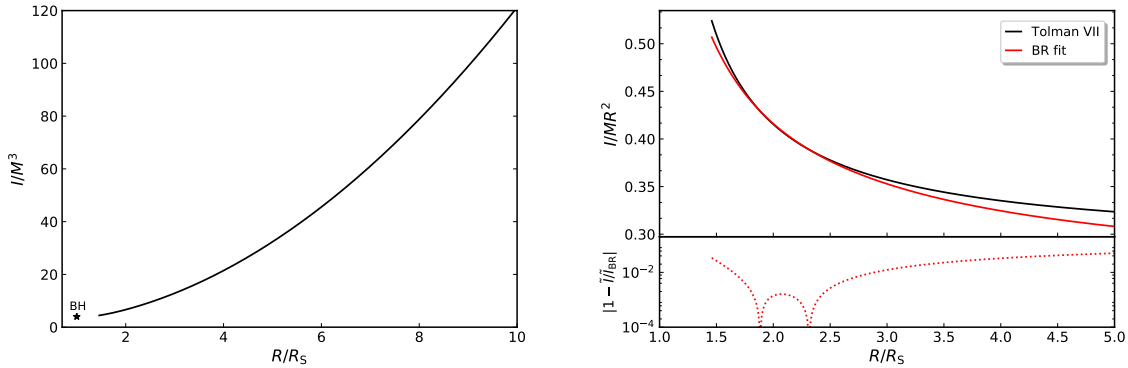


**Figure 4.** *Moment of inertia for the T-VII solution.* **Left panel:** Dimensionless moment of inertia  $\tilde{I} = I/M^3$ , as a function of the tenuity  $R/R_S$ . The star indicates the black hole (BH) value  $\tilde{I} = 4$ . **Right panel:** normalized moment of inertia  $I/(MR^2)$  plotted as a function of the stellar tenuity  $R/R_S$  (solid black line). We also include the polynomial fit proposed by [54] for realistic EOS of NSs (solid red line). The bottom panel shows the relative error.

as  $\beta \rightarrow 1$ . For instance, for the limiting value for stability  $\beta_{\text{stab}}$  we obtain  $\tilde{I} = 4.460$ . Notice however that the strict BH limit ( $\beta \rightarrow 1$ ), cannot be taken from this solution, or any other EOS for realistic NSs, for any finite value of the central energy density  $\S$ .

It has been suggested by some authors [12, 55, 56, 57] that the normalized moment of inertia  $I_{\text{norm}} \equiv I/MR^2$ , for stars in slow rotation, can be expressed as a function of the compactness of the configuration  $\mathcal{C} \equiv M/R$ , through some relatively simple low-

$\S$  It has been shown that, under certain conditions, uniform density stars can evade the Buchdahl bound and approach arbitrarily close to the BH compactness limit where they become essentially a gravastar [50, 51]. Moreover, in this limit, quantities like the Love number, normalized moment of inertia, and quadrupole moment, approach the corresponding Kerr values [52, 53].

order polynomial functions which have a mild dependence on the EOS. For instance, by considering a number of EOS for realistic NSs, [58] proposed a quartic order polynomial fit given by

$$I_{\text{norm}} = \tilde{a}_0 + \tilde{a}_1 \mathcal{C} + \tilde{a}_4 \mathcal{C}^4, \quad (4.1)$$

with the following fitting coefficients,  $\tilde{a}_0 = 0.237 \pm 0.008$ ,  $\tilde{a}_1 = 0.674$  and  $\tilde{a}_4 = 4.48$ . More recently, [54] considered a larger number of EOS for realistic NSs in a wide range of compactness, namely,  $\mathcal{C} \in [0.07, 0.32]$ . They found that the fitting coefficients are  $\tilde{a}_0 = 0.244$ ,  $\tilde{a}_1 = 0.638$  and  $\tilde{a}_4 = 3.202$ .

In the right-hand panel of figure 4 we plot the same results as in the left-hand panel but now normalized as  $I/MR^2$ , for various values of the tenuity parameter  $R/R_s$ . Note that as the tenuity decreases, or the compactness increases,  $I_{\text{norm}}$  grows monotonically approaching a value above 0.5, when  $\beta$  approaches the limiting value for dynamical stability. In order to compare the predictions for  $I_{\text{norm}}$  of the T-VII solution with those of realistic EOS for NSs, we include the fitting polynomial formula (4.1) with the coefficients reported by [54]. In the bottom panel we show the relative error. We observe that the greatest differences appear for  $\beta > 3.5$  where the relative errors are above 5%, while the agreement improves significantly in the range  $1.63 < \beta < 2.9$ , which roughly speaking is the relevant range of compactness for realistic NSs [33], where the relative error is below 1%. Thus, these results suggest that, in terms of the normalized moment of inertia, the T-VII solution provides a very good description of a realistic NS in the relevant regime.

#### 4.2. Spherical deformations: $l = 0$ sector

The surface value of the deformation parameter  $\xi_0/R$  (2.31), as a function of the tenuity  $\beta$ , is plotted in figure 5. We observe that  $\xi_0$  is not monotonic; instead, as  $\beta$  decreases  $\xi_0$  increases reaching a local maximum at  $\beta \simeq 3.7$ , and then it decreases approaching zero as  $\beta \rightarrow \beta_{\text{stab}}$ . Similar behaviour was found for homogeneous stars in slow rotation, but the maximum there appears at  $\beta \sim 3.3$  [41].

The fractional change of mass  $\Delta M \equiv \delta M/M$ , as given by (2.16), is shown in figure 6 as a function of the tenuity  $R/R_s$ . It is worthwhile to recall that in the T-VII solution, the energy density vanishes at the surface, thus the last term on the right-hand side of (2.16) does not contribute to  $\delta M$ . We observe that  $\Delta M$  is not monotonic, instead, it grows as  $\beta$  decreases reaching a maximum at  $\beta \sim 3.19$ , and then it decreases as  $\beta \rightarrow \beta_{\text{stab}}$ . Similar behaviour was also found for constant density stars, where the maximum of the function  $\Delta M$  was found at  $\beta \sim 2.8$  [43].

#### 4.3. Quadrupole deformations: $l = 2$ sector

In figure 7 we display the deformation function  $-\xi_2(R)/R$ , as given by (2.32), evaluated at the surface, as a function of the tenuity parameter  $\beta$ . In analogy to the behaviour of the  $l = 0$  perturbation function  $\xi_0$ , as  $\beta$  decreases, or the compactness increases,

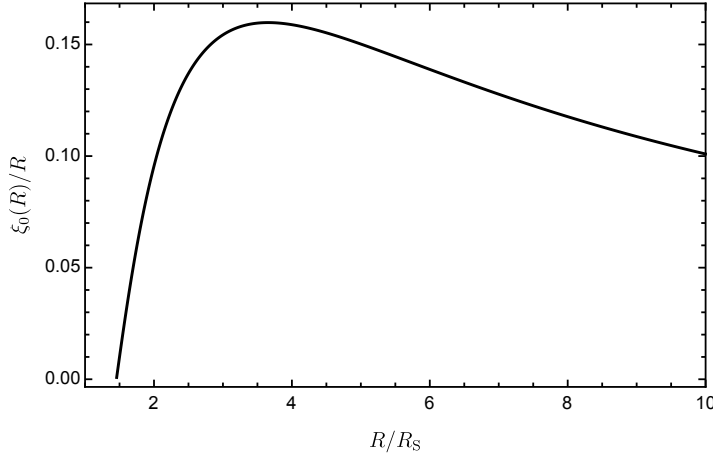


**Figure 5.** The  $l = 0$  deformation of the surface  $\xi_0/R$  (measured in units of  $(J/M^2)^2$ ) as a function of  $R/R_S$ .

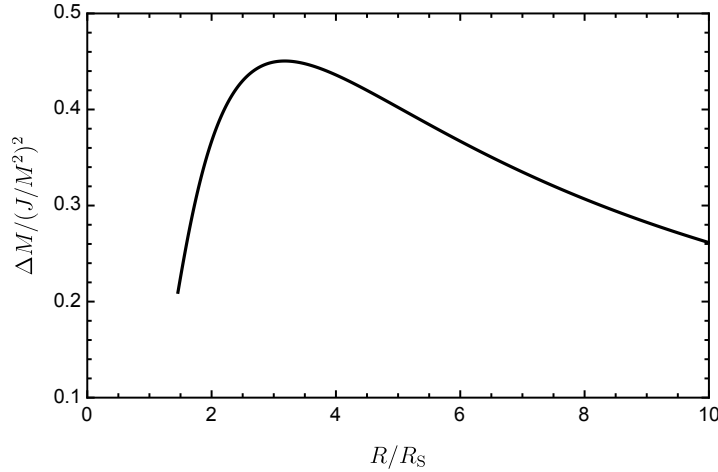


**Figure 6.** The fractional change of mass  $\Delta M$  against the parameter  $R/R_S$ ;  $\Delta M$  is measured in units of  $(J/M^2)^2$ .

$-\xi_2(R)/R$  increases reaching a maximum at  $\beta \simeq 2.95$ , and then decreases as  $\beta \rightarrow \beta_{\text{stab}}$ . This behaviour for  $-\xi_2(R)/R$  was also found for homogeneous stars where the maximum appears at  $\beta \sim 2.7$  [41].

The radial profile of the ellipticity  $\varepsilon(r)$  of the isobaric surfaces, as given by (2.34), is illustrated in figure 8, for various values of the tenuity  $\beta$ . We measure  $\varepsilon(r)$  in units of  $(J/M^2)^2$ . We observe that the ellipticity grows monotonically from the centre of the star, up to the surface. Also, note that for configurations with low compactness, the region  $r/R \in (0, 0.6)$  is less deformed as compared with the region  $r/R \in (0.6, 1)$ . For instance, for the configuration with  $\beta = 10$ , equivalent to  $\mathcal{C} = 0.05$ , the ellipticity is almost constant up to  $r/R \sim 0.6$ , and then it grows rapidly in the region  $r/R \in (0.7, 1)$ . On the other hand, for the configuration with the limiting  $\beta$  for stability, we observe that the ellipticity grows almost linearly, and slowly, with  $r$ , thus the inner and outer cores deformations are comparable.

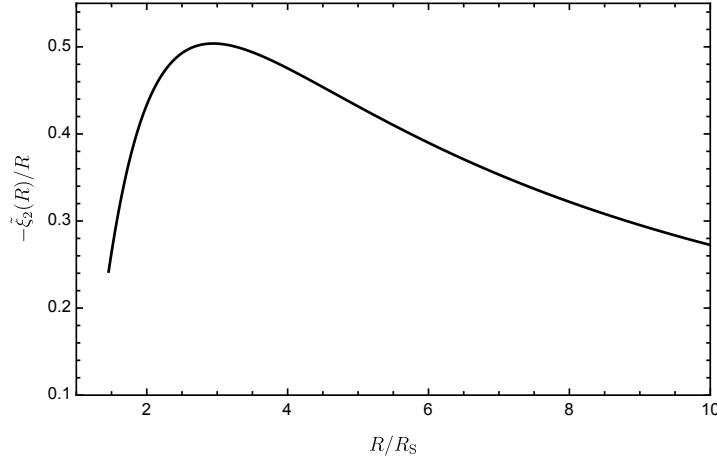


**Figure 7.** The  $l = 2$  deformation of the surface  $\xi_2(R)/R$  (measured in units of  $(J/M^2)^2$ ) as a function of  $R/R_S$ .

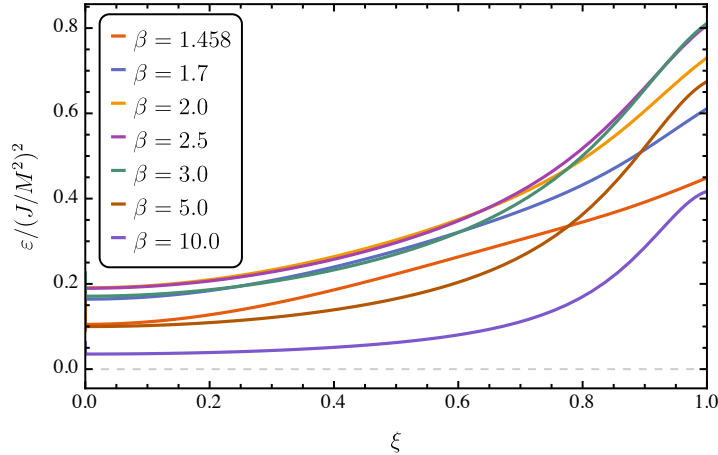


**Figure 8.** Radial profile of the ellipticity  $\varepsilon(r)$ , in units of  $(J/M^2)^2$ , for various values of the tenuity  $R/R_S$ .

The ellipticity of the bounding surface  $\varepsilon_1$ , as a function of  $\beta$ , is shown in figure 9. We observe that the ellipticity grows as the star increases its compactness while keeping mass and angular momentum fixed; when  $\beta \sim 2.8$  the ellipticity reaches a maximum and then decreases. Thus, when a T-VII spheroid is contracted beyond this point, it will become more spherical than oblate. This reversal in the behaviour of the ellipticity, which is not predicted in Newtonian mechanics, was also found for the Maclaurin spheroids [41], and also for polytropes [44] in slow rotation. Note however that the turning  $\beta$ -point in the ellipticity, for the T-VII spheroids, is a little above  $\beta \sim 2.4$  corresponding to the maximum found for homogeneous stars [41], but it seems to be closer to the maximum found for polytropes with  $\gamma = 5/2$  [44]. In principle, our results support the hypothesis drawn by [44], namely that for a contraction where  $J/M^2$  remains fixed, a maximum in the ellipticity will occur for  $\beta$  in the range 2 to 3 if the EOS allows high dense configurations to exist in hydrostatic equilibrium.

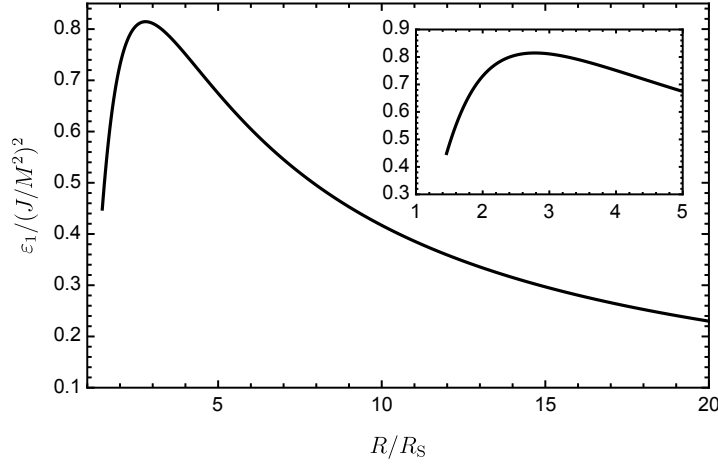


**Figure 9.** The ellipticity of the surface  $\varepsilon_1$  (in units of  $(J/M^2)^2$ ), as a function of the parameter  $R/R_S$ . The inset shows a magnification of the region near the maximum  $\beta \sim 2.8$ , where the ellipticity changes its behaviour.

The explanation of the reversal in the behaviour of the ellipticity follows the main argument given by [44]. Let us recall that the centrifugal effects are due to the angular velocity  $\varpi(r)$ , relative to the local inertial frame. From figure 2 we notice that as the compactness of the star increases,  $\varpi(r)$  is suppressed all along the interior of the star, therefore the centrifugal effects are weakened during the quasi-stationary and adiabatic contraction. Incidentally, we observe from figure 3 the reversal in the behaviour of the surface value  $\varpi_1$ , as the star becomes more compact. Although the maximum there appears at a different value of  $\beta$  from the one where the ellipticity reaches a local maximum, from (2.17) and (2.18) it can be seen that the functions  $h_2(r)$  and  $v_2(r)$  involve  $\varpi$  in a non-trivial manner, thus there is no reason *a priori* to expect that those maxima should coincide.

In figure 10 we plot the ‘Kerr factor’  $\tilde{q} \equiv QM/J^2$  [44], as a function of the parameter  $\beta$ , for the T-VII solution. The Kerr factor is relevant because it gives an account of the deviations of the external Hartle-Thorne metric away from the Kerr spacetime ( $\tilde{q}_{\text{BH}} = 1$ ). We observe that as the compactness increases,  $\tilde{q}$  decreases monotonically and it seems to approach the Kerr BH value as  $\beta$  approaches the limiting value for dynamical stability. For instance, for  $\beta = \beta_{\text{stab}}$ , we obtain  $\tilde{q} = 1.116$  (see table A1). Similar behaviour was also found for a number of realistic EOS for NSs, including polytropes [14, 57]. Thus, these results support the universality of the approach of  $\tilde{q}$  to the Kerr value as the compactness approaches  $1/2$ . However, as we pointed out before, the strict BH limit ( $\beta \rightarrow 1$ ) cannot be considered from this solution or any other realistic EOS for NS, no matter what value of the central energy density is chosen.

By systematically studying the quadrupole moment for various EOS for realistic NSs, [57] found a universal behaviour between  $\tilde{q}$  and the tenuity  $\beta$ , which is almost insensitive of the EOS. Furthermore, they proposed an analytical fitting formula to

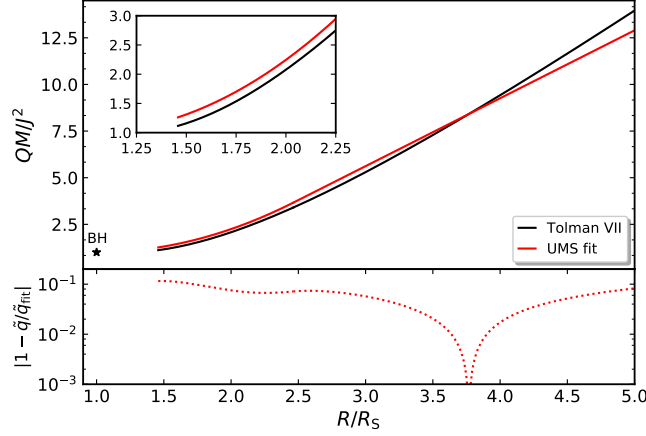


**Figure 10.** The ‘Kerr factor’  $\tilde{q} \equiv QM/J^2$ , as a function of the tenuity  $R/R_S$ , for the T-VII solution (black solid line). We also include the analytic fitting formula (red solid line) for the selected EOS considered in [57]. The star indicates the Kerr BH value  $\tilde{q} = 1$ . The relative error is shown in the bottom panel.

describe this universal behaviour, which takes the form

$$\tilde{q} = \begin{cases} \alpha_1 \beta + \alpha_0, & \beta > \beta_0, \\ \delta(\beta - 1)^2 + 1, & \beta \leq \beta_0, \end{cases} \quad (4.2)$$

where  $\delta = -\alpha_1^2/[4(\alpha_1 + \alpha_0 - 1)]$ , with the fitted coefficients  $\alpha_0 = -5.3$  and  $\alpha_1 = 3.64$ , and  $\beta_0 = 2(1 - \alpha_0)/\alpha_1$  is the matching point.

In order to compare the predictions for  $\tilde{q}$  of the T-VII solution with those for realistic EOSs for NSs, in figure 10 we include the fitting formula (4.2) with the coefficients found by [57] (red solid line). In the bottom panel, we show the relative error. We observe that for  $\beta \gtrsim 4.5$  the relative error is above 5%, but then the agreement improves in the range  $3.11 < \beta < 4.5$ , where the relative error is below 5%. However, for  $\beta_{\text{stab}} < \beta \lesssim 3$  the relative error goes above 5% reaching almost 12% for the limiting value of  $\beta$  for stability. Considering the relevant range for realistic NSs, i.e.  $1.63 < \beta < 2.9$ , relative errors vary between 6% and 10%, which indicates higher deviations in contrast with the results we found for the normalized moment of inertia in that same regime.

## 5. Concluding remarks

In this paper, we have presented an extension to slow rotation of the well-known Tolman VII (T-VII) solution [11]. For this purpose, we have used the Hartle-Thorne perturbative framework at second order in the angular velocity  $\Omega$  [37, 38]. In this approximation, the fractional rotational perturbations are fully determined by the tenuity parameter  $\beta \equiv R/R_S$  and the ratio  $J/M^2$ ; the latter remaining constant for an adiabatic and quasi-stationary collapse, as the one being modelled here. Thus, we integrated the Hartle-Thorne equations for various values of the tenuity  $\beta$ , up to the limiting value

for dynamical stability, and then determined the corresponding surface and integral properties for each model.

Let us summarize our main results. We determined the dimensionless moment of inertia  $\tilde{I} \equiv I/M^3$  and confirmed the results reported by [23], for the T-VII solution. We found that, as the compactness of the configuration increases,  $\tilde{I}$  decreases monotonically and seems to approach the BH value  $\tilde{I} = 4$ , as  $\beta$  approaches the limiting value for stability. We must stress, however, that the strict BH limit, i.e.  $\beta \rightarrow 1$ , cannot be taken from this solution, or any other realistic EOS for NS, no matter what value of the central energy density is chosen. Furthermore, we found that the normalized moment of inertia  $I/MR^2$ , within the relevant regime of compactness for realistic NSs, is in excellent agreement with the numerical results for realistic EOSs of NSs. Thus, in this context, the T-VII provides a very satisfactory description of the interior of a NS.

We determined the ellipticity of the bounding surface for the T-VII spheroids, for fixed mass and angular momentum, and we found a reversal in its behaviour when  $\beta \sim 2.8$ . This seemingly counterintuitive effect, which is not predicted in Newtonian theory, was also found in homogeneous stars [41] and polytropes [44], in slow rotation. This reversal in the ellipticity behaviour can be considered as a purely relativistic effect as a consequence of the intricate interplay of the dragging effects, given by the  $l = 0$  perturbations equations, with the  $l = 2$  quadrupole perturbations. An alternative explanation for the reversal in the behaviour of the ellipticity was proposed by [59, 60]. These authors argue that the reversal could be due to the change in the behaviour of rotational effects in the presence of strong gravitational fields, which occurs even in the absence of dragging effects [61, 62]. We can expect its relation to the reversal of the centrifugal effects in strong gravitational fields as discussed by [63].

Finally, we determined the Kerr factor  $\tilde{q}$  for the T-VII spheroids and found that it decreases monotonically and seems to approach the Kerr value  $\tilde{q} = 1$ , as the compactness tends to the limiting value for stability. We also compared our results with the universal fit for  $\tilde{q}$  proposed by [57] for realistic NSs, which is almost independent of the EOS. In the relevant range of compactness for NSs, relative errors are between 6% and 10%, which are bigger than those we found for the normalized moment of inertia but still within a reasonable margin. Nevertheless, it is worthwhile to remark that despite its simplicity, by having an energy density profile that varies quadratically with the radius  $r$ , the T-VII solution seems to approximate very well to realistic NSs, which are expected to have an intricate interior region, characterized by different layers endowed of gradients of density and pressure.

An alternative to improve the agreement between the T-VII solution and the universal fitting relations for realistic NSs, is to find some suitable modification to the T-VII model. Along this direction, [22] proposed a modified T-VII solution (MT-VII), by including an extra parameter  $\alpha$  that allows the energy density to become a quartic function of  $r$ . These authors showed that this model provides a better agreement, for metric, pressure, and energy density, with the numerical results of realistic EOSs for NSs. However, in [28] we pointed out certain flaws of the MT-VII model, particularly

the prediction of unphysical regions of negative pressure near the stellar surface, for certain values of the parameter  $\alpha$  and compactness  $\mathcal{C}$ . Thus, inspired by the energy density profile introduced by [22], we proposed the ‘exact modified Tolman VII’ (EMT-VII) solution [28], which alleviates the drawbacks of the original MT-VII model. Therefore, a further study would be to consider the EMT-VII model in slow rotation, determine their corresponding normalized moment of inertia and quadrupole moments, and then examine how these compare with the results for realistic EOSs for NSs. It is likely that for certain values of the parameter  $\alpha$  the agreement for  $I$  and  $\tilde{q}$  can improve significantly.

## Acknowledgments

The authors acknowledge the support of the Institute of Physics and its Research Centre for Theoretical Physics and Astrophysics, at the Silesian University in Opava.

## Appendix A. Integral and surface properties of slowly rotating Tolman VII spheroids

**Table A1.** Surface properties of slowly rotating Tolman VII spheroids, for some selective values of the tenuity  $\beta \equiv R/R_S$ . The main results are displayed in the accompanying figures. We employ the same units introduced by [41, 44]. Here we include the corresponding factors  $c$  and  $G$  in case one wishes to recover the physical parameters. The stellar radius is measured in units of the Schwarzschild radius  $R_S \equiv 2GM/c^2$ . The moment of inertia  $I$  is measured in units of  $M^3$ ; the normalized moment of inertia  $I_{\text{norm}} \equiv I/MR^2$  is dimensionless; the change in mass  $\Delta M \equiv \delta M/M$  is measured in the unit  $(GJ/M^2c^3)^2$ ; the ‘Kerr factor’  $\tilde{q} \equiv QM/J^2$  is dimensionless; the surface angular velocity  $\varpi_1$ , relative to the local inertial frame, is measured in the unit  $GJ/M^3c^2$ ; the ellipticity  $\varepsilon$  is measured in units of  $(GJ/M^2c^3)^2$ .

$\beta$	$I/M^3$	$I_{\text{norm}}$	$\Delta M$	$\tilde{q}$	$\varpi_1$	$\varepsilon$
1.459	4.4619	0.5240	0.2098	1.1165	0.1436	0.4486
1.492	4.5598	0.5120	0.2223	1.1507	0.1440	0.4752
1.780	5.6323	0.4444	0.3160	1.5921	0.1332	0.6505
2.104	7.1747	0.4051	0.3852	2.3421	0.1125	0.7557
2.763	11.164	0.3656	0.4438	4.4246	0.0777	0.8144
3.690	18.537	0.3403	0.4440	8.0832	0.0489	0.7736
5.000	32.354	0.3235	0.4021	13.963	0.0289	0.6745

## References

- [1] Schaffner-Bielich J 2020 *Compact Star Physics* (Cambridge University Press)
- [2] Stuchlík Z, Hledík S and Novotný J 2016 *Phys. Rev. D* **94** 103513 (*Preprint* 1611.05327)
- [3] Novotný J, Hladík J and Stuchlík Z 2017 *Phys. Rev. D* **95** 043009 (*Preprint* 1703.04604)
- [4] Posada C, Hladík J and Stuchlík Z 2020 *Phys. Rev. D* **102** 024056 (*Preprint* 2005.14072)
- [5] Yagi K, Stein L C, Pappas G, Yunes N and Apostolatos T A 2014 *Phys. Rev. D* **90** 063010 (*Preprint* 1406.7587)
- [6] Alvarez-Castillo D E and Blaschke D B 2017 *Phys. Rev. C* **96** 045809 (*Preprint* 1703.02681)
- [7] Schwarzschild K 1916 *Sitzungsber. Preuss. Akad. Wiss. Berlin (Math. Phys.)* **1916** 424–434 (*Preprint* physics/9912033)
- [8] Stuchlík Z 2000 *Acta Phys. Slov.* **50** 219
- [9] Boehmer C G 2004 *Gen. Rel. Grav.* **36** 1039–1054 (*Preprint* gr-qc/0312027)
- [10] Buchdahl H A 1967 *Astrophys. J.* **147** 310
- [11] Tolman R C 1939 *Phys. Rev.* **55** 364–373
- [12] Lattimer J M and Prakash M 2001 *Astrophys. J.* **550** 426 (*Preprint* astro-ph/0002232)
- [13] Postnikov S, Prakash M and Lattimer J M 2010 *Phys. Rev. D* **82** 024016 (*Preprint* 1004.5098)
- [14] Yagi K and Yunes N 2013 *Phys. Rev. D* **88** 023009 (*Preprint* 1303.1528)
- [15] Yagi K and Yunes N 2016 *Class. Quant. Grav.* **33** 095005 (*Preprint* 1601.02171)
- [16] Neary N, Ishak M and Lake K 2001 *Phys. Rev. D* **64** 084001 (*Preprint* gr-qc/0104002)
- [17] Tsui L K and Leung P T 2005 *Phys. Rev. Lett.* **95**(15) 151101
- [18] Tsui L K and Leung P T 2005 *Astrophys. J.* **631** 495–505 (*Preprint* gr-qc/0505113)
- [19] Raghoonundun A M and Hobill D W 2015 *Phys. Rev. D* **92** 124005 (*Preprint* 1506.05813)
- [20] Moustakidis C C 2017 *Gen. Rel. Grav.* **49** 68 (*Preprint* 1612.01726)
- [21] Sotani H and Kokkotas K D 2018 *Phys. Rev. D* **97** 124034 (*Preprint* 1806.00568)
- [22] Jiang N and Yagi K 2019 *Phys. Rev. D* **99** 124029 (*Preprint* 1904.05954)
- [23] Jiang N and Yagi K 2020 *Phys. Rev. D* **101** 124006 (*Preprint* 2003.10498)
- [24] Stuchlík Z, Hladík J, Vrba J and Posada C 2021 *Eur. Phys. J. C* **81** 529 (*Preprint* 2106.05750)
- [25] Posada C, Hladík J and Stuchlík Z 2021 *Phys. Rev. D* **103** 104067 (*Preprint* 2103.12867)
- [26] Stuchlík Z and Vrba J 2021 *Eur. Phys. J. Plus* **136** 977 (*Preprint* 2108.09466)
- [27] Yagi K and Stepniczka M 2021 *Phys. Rev. D* **104**(4) 044017
- [28] Posada C, Hladík J and Stuchlík Z 2022 *Phys. Rev. D* **105** 104020 (*Preprint* 2201.05209)
- [29] Pappas T D, Posada C and Stuchlík Z 2022 *Phys. Rev. D* **106** 124014 (*Preprint* 2210.15597)
- [30] Koliogiannis P S, Tsalis G A, Panos C P and Moustakidis C C 2022 (*Preprint* 2206.12138)
- [31] Jayawiguna B N, Prasetyo I, Sulaksono A and Ramadhan H S 2022 *Phys. Rev. D* **106** 104020
- [32] Gendreau K C *et al.* 2016 The Neutron star Interior Composition Explorer (NICER): design and development *Space Telescopes and Instrumentation 2016: Ultraviolet to Gamma Ray* vol 9905 ed den Herder J W A, Takahashi T and Bautz M International Society for Optics and Photonics (SPIE) p 99051H URL <https://doi.org/10.1117/12.2231304>
- [33] Miller M C *et al.* 2021 *Astrophys. J. Lett.* **918** L28 (*Preprint* 2105.06979)
- [34] Riley T E *et al.* 2021 *Astrophys. J. Lett.* **918** L27 (*Preprint* 2105.06980)
- [35] Salmi T *et al.* 2022 *Astrophys. J.* **941** 150 (*Preprint* 2209.12840)
- [36] Paschalidis V and Stergioulas N 2017 *Living Rev. Rel.* **20** 7 (*Preprint* 1612.03050)
- [37] Hartle J B 1967 *Astrophys. J.* **150** 1005–1029
- [38] Hartle J B and Thorne K S 1968 *Astrophys. J.* **153** 807
- [39] Silva H O, Holgado A M, Cárdenas-Avendaño A and Yunes N 2021 *Phys. Rev. Lett.* **126** 181101 (*Preprint* 2004.01253)
- [40] Yunes N, Miller M C and Yagi K 2022 *Nature Rev. Phys.* **4** 237–246 (*Preprint* 2202.04117)
- [41] Chandrasekhar S and Miller J C 1974 *Mon. Not. R. Astron. Soc.* **167** 63–80
- [42] Petroff D 2007 *Class. Quant. Grav.* **24** 1055–1068 (*Preprint* gr-qc/0701081)
- [43] Reina B 2016 *Mon. Not. R. Astron. Soc.* **455** 4512–4517 (*Preprint* 1503.07835)

- [44] Miller J C 1977 *Mon. Not. R. Astron. Soc.* **179** 483–498
- [45] Benitez E, Weller J, Guedes V, Chirenti C and Miller M C 2021 *Phys. Rev. D* **103** 023007 (*Preprint* 2010.02619)
- [46] Reina B and Vera R 2015 *Class. Quant. Grav.* **32** 155008 (*Preprint* 1412.7083)
- [47] Mars M 2005 *Class. Quant. Grav.* **22** 3325–3348 (*Preprint* gr-qc/0507005)
- [48] Alcock C, Farhi E and Olinto A 1986 *Astrophys. J.* **310** 261
- [49] Buchdahl H A 1959 *Phys. Rev.* **116** 1027
- [50] Mazur P O and Mottola E 2015 *Class. Quant. Grav.* **32** 215024 (*Preprint* 1501.03806)
- [51] Posada C and Chirenti C 2019 *Class. Quant. Grav.* **36** 065004 (*Preprint* 1811.09589)
- [52] Chirenti C, Posada C and Guedes V 2020 *Class. Quant. Grav.* **37** 195017 (*Preprint* 2005.10794)
- [53] Beltracchi P, Gondolo P and Mottola E 2022 *Phys. Rev. D* **105** 024002 (*Preprint* 2107.00762)
- [54] Breu C and Rezzolla L 2016 *Mon. Not. R. Astron. Soc.* **459** 646–656 (*Preprint* 1601.06083)
- [55] Ravenhall D G and Pethick C J 1994 *Astrophys. J.* **424** 846
- [56] Bejger M and Haensel P 2002 *Astron. Astrophys.* **396** 917 (*Preprint* astro-ph/0209151)
- [57] Urbanec M, Miller J C and Stuchlík Z 2013 *Mon. Not. R. Astron. Soc.* **433** 1903 (*Preprint* 1301.5925)
- [58] Lattimer J M and Schutz B F 2005 *Astrophys. J.* **629** 979–984 (*Preprint* astro-ph/0411470)
- [59] Abramowicz M A and Miller J C 1990 *Mon. Not. R. Astron. Soc.* **245** 729
- [60] Gupta A, Iyer S and Prasanna A R 1996 *Class. Quant. Grav.* **13** 2675–2682 (*Preprint* gr-qc/9603055)
- [61] Abramowicz M A and Prasanna A R 1990 *Mon. Not. R. Astron. Soc.* **245** 720
- [62] Abramowicz M A 1990 *Mon. Not. R. Astron. Soc.* **245** 733
- [63] Abramowicz M A, Miller J C and Stuchlík Z 1993 *Phys. Rev. D* **47** 1440